



# Effect of Underreamed Pervious Concrete Columns on Load-Carrying Capacity of Loose Cohesionless Soils

Sudheer Kumar Jala<sup>1</sup>; Saurabh Rawat<sup>2</sup>; and Ashok Kumar Gupta<sup>3</sup>

**Abstract:** Weak confinement governs the bulging failure of granular columns. Pervious concrete columns have granular columns like drainage with stiffness of concrete column are thus independent of the confinement from the weak surrounding soil can be treated as an alternative solution. Moreover, it is well established that under-reaming bulb enhances the bearing resistance to the pile shaft. Therefore, the present experimental and analytical study investigates circular pervious concrete column (CPCC) and under-reamed pervious concrete column (UPCC) in improving the bearing capacity of loose pond ash fill. CPCC and UPCC are constructed in a model pond ash fill subjected to vertical loading. The load-carrying capacity, settlement failure mechanism, and consolidation parameters were examined. Theoretical analysis for evaluating the load-carrying improvement factor (LCF) with nondimensional parametric variation of area replacement ratio ( $R_a$ ), underreamed bulb ratio ( $B_r$ ), and length ratio of the column ( $R_L$ ) was also done. Efficacy of CPCC was also numerically studied (Plaxis 3D). Experimental results show that the vertical settlement is reduced by 52.8% with CPCC and UPCC. UPCC renders higher load-carrying capacity than CPCC. Both CPCC and UPCC undergo deformation at depth of 4D during failure. For the same area replacement ratio ( $R_a$ ), the experimental and theoretically computed values are found in good agreement. The rate of consolidation is reduced from 53 to 23 days by using CPCC signifying its drainage potential. DOI: 10.1061/IJGNAI.GMENG-7659. © 2022 American Society of Civil Engineers.

**Author keywords:** Pervious concrete column; Underreamed; Pond ash; Bulb ratio; Plaxis 3D; Consolidation.

## Introduction

In India, more than 40,000 ha (CRRRI 2019) of land is occupied by industrial waste ash fills. The fill sites of Delhi, Mumbai, Kolkata, and Chennai itself occupies about 228,400 ha (Gupta et al. 2015) of the subcontinent. Due to the large fill depth of 4–30 m, shallow depth treatment for improvement of these sites becomes ineffective for moderate to heavy loaded structures. Furthermore, due to the large lateral spread of the fill area, ground improvement using admixtures becomes costly. Thus, for a disposed material with low cohesion, smaller unit weight than silt or sand, and poor load-carrying capacity due to weak confinement can best be improved by using stone columns. Though the granular stone columns increased the rate of consolidation and bearing capacity and decreased the liquefaction potential and settlement of poor soil condition, the bulging failure mechanism of a typical granular stone columns occurring about two–three times the column diameter from the ground level was governed by confinement provided by the surrounding soil. Utilization of granular stone columns in very poor soils is generally limited owing to the minimum lateral confinement provided by the surrounding soil against bulging failure (Barksdale and Bachus

1983; Bergado et al. 1994; Suleiman et al. 2014). To overcome this issue, researchers incorporated the concept of partial or full encasement of the granular columns using geosynthetics to enhance the stiffness (Murugesan and Rajagopal 2006, 2010; Khabbazian et al. 2010; Alexiew and Raithel 2015; three Chen et al. 2021; Zhang and Zhao 2015; Kumar et al. 2020; Mohapatra and Rajagopal 2017; six Cengiz and Güler 2018; seven Hosseinpour et al. 2019; Thakur et al. 2021a, b, c). The encapsulation of granular columns minimized the squeezing of column material into the surrounding soil and limited the bulging only up to a certain extent. Likewise, researchers such as Golait and Padade (2017, 2018) employed cemented stone columns for increasing the stiffness of the granular material that converted the bulging failure into a pronounced punching failure but with a compromised column permeability. Therefore, to achieve a punching dominant failure mechanism with significant permeability, Suleiman et al. (2014) developed a pervious concrete column with an average porosity of 20%, permeability of 1.33 cm/s, and 28-day compressive strength of 18.3 MPa, resulting in an unconfined compressive strength of 10 times more than that of the confined granular columns. Moreover, the pervious concrete pile-reinforced surface reduced the peak horizontal acceleration amplification by 57% versus 27% as obtained by granular piles (Zhang et al. 2017). The installation of pervious concrete pile (PCP) using a vibrating sinking tube significantly improved the bearing capacity of surrounding soil, reduced the excess pore water pressure, and increased the pile–soil stress ratio, and depicted reduced lateral displacement (Qing et al. 2021; Zhang and Zhao 2015). The flexural strength of the pervious concrete columns decreases in the order of ternary, binary, and single material mixture, varying in the range of 1.5 to 3.2 MPa (Chandrappa and Biligiri 2018). The cast in situ PCPs also showed higher bearing capacity than did precast PCPs because of larger mobilization of frictional stresses during installation. In addition, inclusion of a bulb at 0.4 to 0.6 times the length of the pile is found to provide the maximum resistance in cohesionless soil (Prakash and Ramakrishna 2004). Golait and Padade (2018) also showed that using underreamed cemented stone

<sup>1</sup>Research Scholar, Dept. of Civil Engineering, Jaypee Univ. of Information Technology, Solan, Himachal Pradesh, India. Email: sudhiriitd@gmail.com

<sup>2</sup>Assistant Professor, Dept. of Civil Engineering, Jaypee Univ. of Information Technology, Solan, Himachal Pradesh, India (corresponding author). ORCID: <https://orcid.org/0000-0002-0678-8244>. Email: saurabh.rawat@juit.ac.in

<sup>3</sup>Professor, Dept. of Civil Engineering, Jaypee Univ. of Information Technology, Solan, Himachal Pradesh, India. ORCID: <https://orcid.org/0000-0002-8996-2374>. Email: ashok.gupta@juit.ac.in

Note. This manuscript was submitted on January 16, 2022; approved on September 21, 2022; published online on December 21, 2022. Discussion period open until May 21, 2023; separate discussions must be submitted for individual papers. This paper is part of the *International Journal of Geomechanics*, © ASCE, ISSN 1532-3641.

columns, the bearing capacity improvement factor  $F_b$  increases by 45%–50% in comparison with straight-shafted cemented stone columns with an enlarged bulb located at a depth of five times the column diameter.

Thus, it can be summarized from the literature review that in soil conditions without significant lateral confinement, stone columns with high stiffness (independent of the confinement) and having drainage characteristics such as granular columns with increased end-bearing resistance against punching can be treated as a feasible solution. Based on this, the present research work aims to accomplish the following objectives:

1. To experimentally evaluate the load-carrying capacity, settlement, failure mechanism, and consolidation parameters of pond ash fill reinforced using circular pervious concrete column (CPCC) without bulb and underreamed pervious concrete column (UPCC) with bulbs.
2. To theoretically analyze the reinforcing mechanism of CPCC and UPCC, determine the load-carrying improvement factor (LCF) with nondimensional parametric variation of area replacement ratio ( $R_a$ ), underreamed bulb ratio ( $B_r$ ), and length ratio of the column ( $R_L$ ) and propose equations with experimental validation.
3. To examine the efficacy of CPCC by evaluating the rate of change of consolidation of an embankment supported on CPCC embedded in pond ash fill through finite-element numerical study using Plaxis 3D.

To achieve these objectives, a pervious concrete mixture was prepared, and ash pond fill condition was set up in a test tank. The ash pond fill was reinforced using two different types of columns: (a) CPCC without bulb, and (b) underreamed UPCC with a single bulb. Both the CPCC and UPCC were thus subjected to a gradually increasing axial loading. The load-carrying factors were determined from the theoretical analysis and the reinforcing scenarios were also studied for parametric variations of area replacement ratio, bulb ratio, and column lengths ratio. The experimental results were also validated with the analytical results. Two cases of an embankment resting on untreated pond ash fill and improved pond ash fill using CPCC were also investigated to evaluate the efficacy in terms of rate of change of consolidation and dissipation of excess pore water pressure using Plaxis 3D. The present study examines the performance of CPCC and UPCC for its drainage and bearing-capacity improvement criteria.

## Materials

### Pond Ash

Pond ash was collected from the thermal power plant, Ropar, Punjab, India. The preliminary physical parameters were tested in accordance with the Bureau of Indian Standards (BIS) for recording the various geotechnical properties of pond ash (PA), as summarized in Table 1 (Kumar and Sharma 2018). The grain size distribution of ash fill varied from 0.075 to 2 mm (Fig. 1).

### Geosynthetic Material for Encasement

The geosynthetics were used as horizontal circular discs within the column at a vertical spacing of  $1.5d$ . The tensile stiffness strength of the biaxial geogrid was 30 kN/m. The horizontally placed circular geosynthetics discs provided shearing resistance on the top and bottom geosynthetic–aggregate interface, which contributed to arresting the lateral displacement of aggregates into the surrounding soil under axial loading (Thakur et al. 2021c).

**Table 1.** Physical properties of ash fill

Property	PA values
$D_{10}$ (mm)	0.2
$D_{30}$ (mm)	0.31
$D_{60}$ (mm)	0.43
$C_u$	2.15
$C_c$	1.12
Max. dry density ( $\text{kN/m}^3$ )	10.2
Min. dry density ( $\text{kN/m}^3$ )	7.7
Dry density ( $\text{kN/m}^3$ )	9.7
Optimum moisture content (%)	35
Coeff. of permeability (cm/sec)	0.00086
Cohesion, $c$ , ( $\text{kN/m}^2$ )	0.33
Angle of internal friction ( $\phi$ ) in ( $^\circ$ )	32

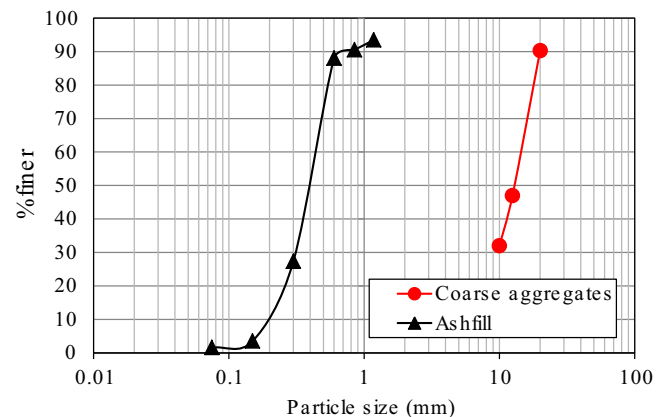


**Fig. 1.** Particle size distribution analysis for surrounding ash fill (pond ash) and coarse aggregates used in pervious concrete.

## Mix Proportions of Pervious Concrete

**Ordinary Portland Cement (OPC 53 Grade).** Coarse aggregates. Based on the reported literature (Suleiman et al. 2014; Golait and Padade 2018; Chandrappa and Biligiri 2018), the pervious concrete was prepared with a water/cement ratio of 0.3 and aggregate/cement ratio of 5 and used uniform graded single-sized particles (Fig. 1) passing through the 12 mm and retained on 10 mm. The specific gravity and water absorption of the aggregates was found to be 2.66 and 5.2, respectively. The aggregate size ranging between 4.75 to 9.5 mm was employed in the field for installation of pervious concrete piles as per the existing literature reported by Qing et al. (2021) and Zhang et al. (2016). Likewise, aggregates of a size classified as poorly graded gravel was used for casting of the recycled aggregate porous concrete pile (Kim et al. 2012). It was also reported that beyond the 7 mm, the effect of aggregate size on compressive strength is negligible (Yu et al. 2019), however using smaller aggregate size decreases the permeability of the pervious concrete (Hung et al. 2021). Hence, with the main objective of having drainage similar to granular piles and sufficient compressive strength to have a column stiffness independent of the confinement from the surrounding weak soil, a larger aggregate size between 10–12 mm was used. As per Wood et al. (2000), for all practical purposes the ratio of column diameter ( $D$ ) to aggregate size ( $d$ ) should be between 12–40 for stone columns. From the published literature (Qing et al. 2021; Zhang et al. 2016) for pervious concrete columns,  $D/d$  ratio of 50–120 is found acceptable. Based on the lower limit of  $D/d$  ratio, for aggregate size between 10–12 mm, the pervious concrete column diameter of 500 to 600 mm could be constructed and installed. This range of diameter lies within the acceptable column

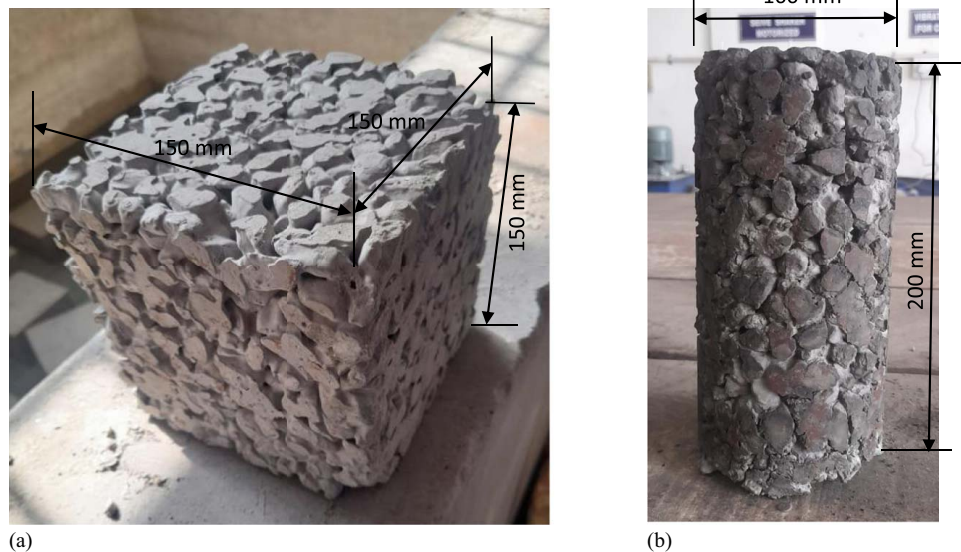


**Fig. 2.** Specimens tested for pervious concrete properties: (a) cube; and (b) cylinder.

diameter range of 0.3 to 0.5 m as recommended by DB37/T 5214-2018 (CBMP 2018) for all practical purposes.

Fine aggregates were purposely omitted in the mix proportion to create large, open porous concrete. After mixing the components, the mixture was placed in the cubic mold (150 × 150 × 150 mm) [Fig. 2(a)] and cylindrical mold of 100 mm in diameter and a length of 200 mm [Fig. 2(b)]. The concrete mixture was placed in layers: three for cubes and four for cylinder. Each layer was compacted with a standard proctor rammer by giving 20 blows to each layer uniformly. Each layer of the pervious concrete column was compacted with a 12-mm tamping rod. The energy applied to compact the PCC was about 52.26 J, corresponding to the mass of 12 mm rod giving 20 blows on each layer with a fall of 30 mm. The tamping time of 10 s was adopted as per as Suleiman et al. (2014), which renders adequate compressive strength and permeability without segregation of cement paste and aggregates during the compaction and after the removal of the column. After 24 h, the specimen was removed from the mold and placed in a curing tank. The strength tests were performed on cured concrete to calculate the compressive strength of pervious concrete. The compressive strength was found to be 16 MPa at 28 days, with a permeability “*k*” of 1.24 cm/s and split tensile strength of 2.19 MPa.

#### Load–Settlement Tester Tank

The load–settlement tester tank (shown in Fig. 3) was used for model testing and determining the load–settlement of the PCC-supported pond ash fill under vertical loading. The setup was made up of mild steel having a length of 1,200 mm, width 1,000 mm, and depth of 630 mm. The depth and size of the tank were certain to take care of the boundary effects. The size of the tank was more than six times the diameter of the test column (Ali et al. 2014). The four sides and bottom of the tank were made of 12-mm-thick mild steel plates and were stiffened laterally with steel angles on the outer surface to achieve essential stiffness against bending during the tests. The inner surface of the tank walls was coated with silicon grease to minimize friction and boundary effects. The rainfall technique was used to fill the tester tank with pond ash having an average relative density is 40%. The tank was filled in layers of 100 mm, with regular determination of dry unit weight being carried out using a nuclear density meter.

#### Installation Methodology

##### Circular Pervious Concrete Column (CPCC)

Previous studies (Suleiman et al. 2014; Ni et al. 2016; Munaga et al. 2020) on pervious concrete columns had utilized the technique of cast-in-situ casing method that had been employed for installation of sand columns. Similarly, the pervious concrete column of the present study was also installed using an external pipe casing and subsequently casting the concrete column. Suleiman et al. (2014) and Ni et al. (2016) used the method of driving a hollow steel mandrel in a sand tank having a relative density of 32%. The pervious concrete column was cast with the help of a PVC pipe with an inner diameter of 75 mm used as a casing. For conventional stone columns, the diameter is generally varied from 0.6 to 1 m (Wood et al. 2000), and a diameter of up to 1 m is usually recommended for encased stone columns (ESC). In the case of CPCCs, a diameter of 0.3 to 0.5 m is recommended by DB37/T 5214-2018 (CBMP 2018) for all practical purposes. From the literature review for all lab studies, L/D ratio ranges between 2–12 and similitude ratio of 1/4.5 to 1/5 has been adopted for model studies on pervious concrete columns (Munaga et al. 2020; Cai et al. 2021). Therefore, scaling down the recommended diameter for practical purpose by using ratio of diameter (model)/diameter (prototype) equal to 1/5, a CPCC diameter of 75 mm was chosen. The length of the pervious column used was determined for L/D ratio of 7. The calculated value gives a length of 525 mm, but since the soil depth in the tank was 530 mm, the column length was rounded off to 530 mm, which yielded an L/D ratio of 7.06. However, the L/D ratio adopted is well within the range as adopted by previous researchers for CPCC model testing (Table 2).

Hence, the model pervious concrete column with a diameter of 75 mm and length of 530 mm (Fig. 3) corresponds to prototype column of diameter 375 and 2,650 mm length. It can be seen from Table 2 that a similar dimension has been employed in the field for similar soil conditions, which signifies that the adopted dimensions are practical and economical.

Furthermore, construction of pervious concrete columns (PCC) in industrial waste, such as the pond ash, will be inert to the chemical attack due to the fact that concrete is generally attacked by sulphate and sulfuric acid occurring naturally in soils, corrosive chemicals present in industrial waste fills, organic acids, and carbon dioxide present in ground water. The percentage of sulphate, sulfuric acid,

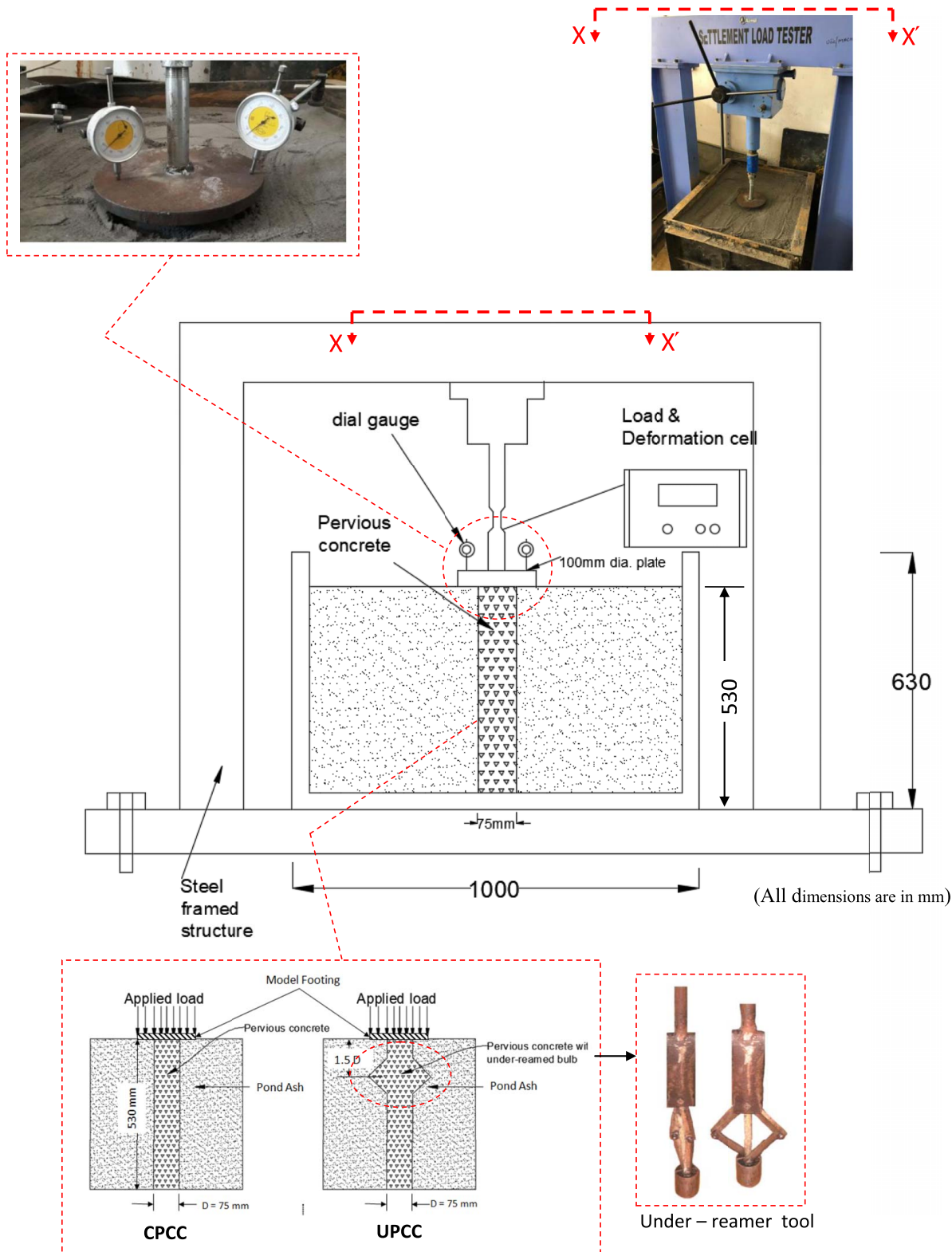


**Fig. 3.** Load–settlement model tank with circular steel plate and dial gauges for testing of CPCC and UPCC along with the used underreaming tool.

and dissolved carbon dioxide presented in the pond ash were found in an insignificant portion of less than 0.5% (Harle 2019; Andhra Pradesh Power Generation Corporation Ltd 2019; Sonawane and Dwivedi 2013; Kumar and Sharma 2018; Bhatt et al. 2019). Therefore, the reaction between concrete and pond ash due to sulphate and sulphate-generated compounds was negligible. In addition, due to the absence of steel reinforcement bars in the employed concrete

columns, the chances of corrosive action on concrete columns were eliminated.

The open-ended PVC is driven into the ash-fill bed and the soil within the casing was removed by using an auger. The prepared pervious concrete mixture was then placed within the PVC casing in layers of 50 mm in thickness, with each layer being compacted well with a 12-mm-diameter tamping rod. When the pervious

**Table 2.** Summary of adopted pervious concrete column/pile dimensions for different soil types from published literature

S. No.	PCC diameter "D" (mm)		PCC length "L" (mm)		Soil Type	L/D ratio	Study scale	Reference
	75	530						
					Pond ash	7.06	Lab	Present study
1	600	1,000			Silt	1.66	Field	Zhang et al. (2016)
2	500	10,000			Silt, silty clay, and silty sand	20	Field	Qing et al. (2021)
3	76	864			Sand	11.36	Large	Suleiman et al. (2014)
	102	1,219				11.95		
4	102	1,321			Sand	12.95	Large	Ni et al. (2016)
5	125	430			Clay	3.44	Lab	Kim et al. (2012)
6	76	916			Sand	12	Lab	Lin et al. (2016)
7	50	300			Sand	6	Lab	Munaga et al. (2020)
8	70	500			Silt	7.2	Lab	Cai et al. (2021)
9	50, 70, 90	100 to 720			Clay	2–8	Numerical	Rashma et al. (2021)

column attained the desired length, the PVC casing was retrieved gradually. The driving of the casing lead to vibrations that disturbed the surrounding soil and simultaneously increased its relative density. Since PVC casing pipe was used, there was no issue of mixing of surrounding pond ash and pervious concrete during construction. After the formation of the column PVC casing was gradually retrieved, filling of the surrounding voids might have occurred. However, this mixing occurs only in the space created by the soil displaced due to the casing thickness (cavity expansion), as also reported by Suleiman et al. (2014).

The top surface of the soil was leveled, and the loading plate was placed flush to the column top. A dial gauge with a magnetic base was attached to the tank and the needle was touched with the loading plate (Fig. 3). Each rotation of the dial gauge reading corresponded to a 1-mm settlement.

### UPCC

The pervious concrete column of shaft diameter 75 mm was bored-cast in the model tank using the replacement method. An underreamed bulb was provided at a depth of 1.5D (D = diameter of the shaft) from the top of the column having a diameter of 2D. The borehole of the required geometry was made with the help of an auger. The underreaming tool with its bucket arrangement (Fig. 3) was lowered into the excavated borehole. The underreamed tool was fixed in level and rotated gently while pressing the handle at the top so that the collapsible sharp edges opened at the required position. The handle was rotated to cut the fill material and form a small bulb-cavity. The cut soil was collected in the bottom bucket and the entire assembly was shrunk to its closed condition and retrieved gradually. The operation was repeated until the required geometry of the bulb was formed. The prepared pervious concrete mix was poured into the borehole in layers (each layer thickness was less than 50 mm) and compacted with the tamping rod. Due to the collapsing tendency of the walls of the bulb, a clay slurry was used to stabilize the excavated shape of the bulb and column walls, thus contributing significantly to the difficulties encountered during preparation of the underreamed columns. The pouring of pervious concrete replaced the clay slurry, but the authors believe that complete replacement of the slurry was difficult to attain due to the complex shape of the UPCC, which resulted in a bulb with slight irregularity. However, after a few trials and failures, satisfactory construction of the UPCC was achieved.

### Loading Sequence and Instrumentation of CPCC and UPCC

The CPCC and UPCC were subjected to vertical load using a model footing plate of 100 mm in diameter and 25 mm in thickness. The diameter of the footing was kept larger than the diameter of the columns so that the load fully occupied the column tributary area and was applied on the composite bed as well. Boundary effects were also verified through the 2V:1H method of footing load distribution.

It was observed that the required tank width at the depth of 0.6 m should be 0.8 m, which is within the available tank width of 1.0 m at the same depth, and, hence, boundary effect is considered as negligible. The model footing was connected through a hydraulic jack which was operated manually by turning the loading wheel clockwise for applying the gradual vertical load (Fig. 3). The axial vertical load was recorded using a load cell of capacity 100 kN and resolution 0.01 N accuracy. Dial gauges with a magnetic base were used to measure the settlement of the footing. A separate load recording cell was attached to the hydraulic system that gave the load and vertical deformation values [Fig. 5(a)]. The least count of the dial gauges and load cell was 0.01 mm. The dial gauges can measure up to 40 mm of maximum vertical displacement. The load in kN corresponding to the unit rotation of the dial gauge was recorded from the load cell attached. The load–settlement behavior was recorded at an interval of 3 and 7 days for different columns.

### Experimental Test Results and Discussions

The area replacement ratio ( $R_a$ ) of 12.3% and column length to diameter ratio is 7, and the pervious concrete column (PCC) with circular cross section and UPCC were tested in the model tank under the 200-mm-diameter circular steel plate. The experiments were carried out after 3 and 7 days of curing of both the CPCC and UPCC samples. The results of the three-day testing are shown in Fig. 4(a). Fig. 4(a) shows the load–settlement ratio relationship at 3 days after construction. It is evident from the figure that UPCC depicts higher load bearing than PCC at any settlement ratio ( $S/D_c$ ) (where  $S$  = total displacement and  $D_c$  = diameter of the column). The initial portion of the curve was almost linear, signifying the direct proportionality between axial load and settlement ratio. The enlarged bulb (UPCC) case rendered 68% higher load-carrying capacity than did the PCC, at a settlement ratio of 40%. The reason for this increased load-carrying capacity of UPCC can be accounted for by the location of the enlarged bulb (i.e., 1.5D), which lay within the failure zone (plastic zone). The identification of the plastic zone was based on the depth at which bulging failure of the ordinary stone columns traditionally occurs. The constant increasing load capacity with the settlement behavior of the curve depicts the improved stiffness of the pond ash–column system. The results are in accordance with the load–settlement behavior of cemented stone columns as reported by Golait and Padade (2018). The stiffness of the composite pond ash–column system was found to be 116 and 213 kN/m for PCC and UPCC, respectively. It was observed that the load-carrying capacity increased by 25% from 3-day to 7-day intervals in each case.

It was observed that at the later stages of loading, a higher load capacity was obtained for UPCC than for PCC. From Fig. 4(b), note that at the vertical settlement ratio of 40 mm, UPCC resisted 63% more load than did PCC. It was observed that up to a settlement

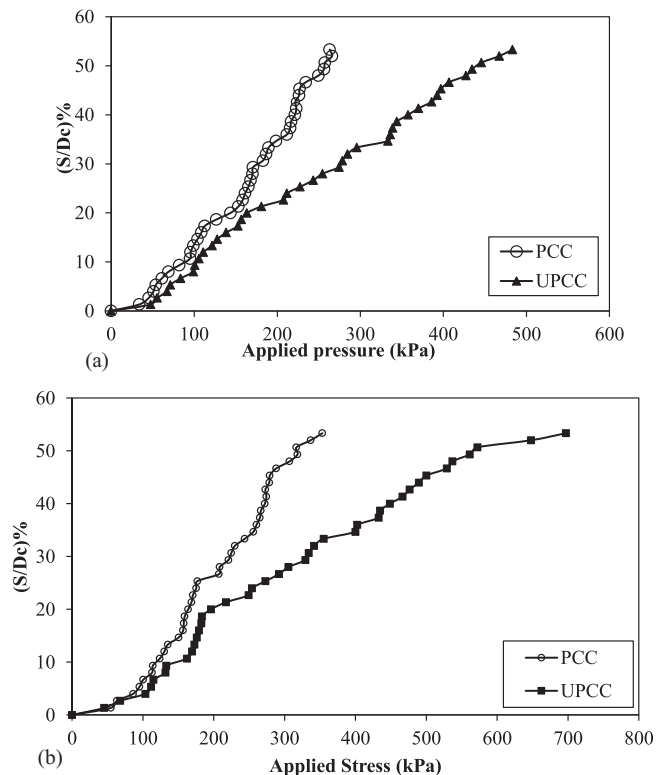


**Fig. 4.** Load settlement behavior of CPCC and UPCC treated soil at (a) 3 days; and (b) 7 days.

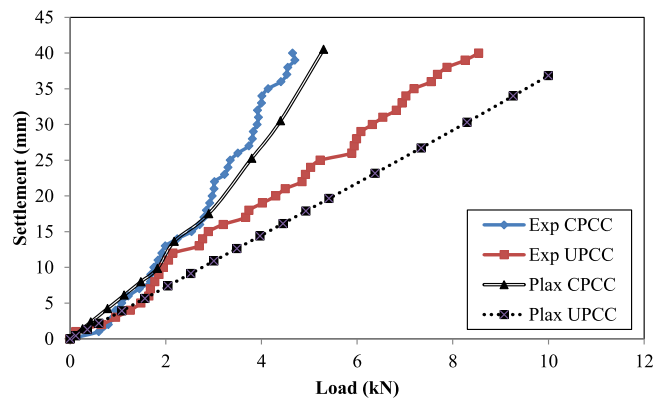


**Fig. 5.** Validation of experimental results with numerical (Plaxis 3D) results.

ratio of 20 mm, both PCC and UPCC followed a similar trend. However, beyond 20 mm, UPCC rendered more bearing capacity and at a lower settlement ratio. The higher load capacity obtained for 7-day testing can be accounted for due the curing time, pozzolanic reaction, and increase of stiffness. The stiffness of the composite pond ash-column system calculated after 7 days of testing was obtained as 156 and 308 kN/m for PCC and UPCC, respectively. Similar kinds of characteristic for cemented stone columns were also reported by Golait and Padade (2018).

#### Validation of Experimental Results with Numerical Methods (Plaxis 3D)

The details of numerical simulation of embedded CPCC in pond ash domain using Plaxis 3D are given in the section for

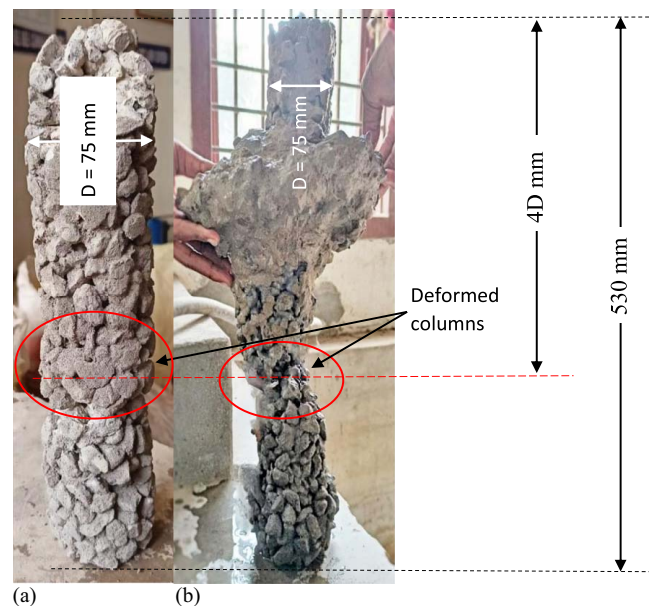


**Fig. 6.** Failure of (a) CPCC; and (b) UPCC.

consolidation studies using 3D numerical study. The results obtained in the numerical modeling were compared with the experimentally measured values, and the same is presented in Fig. 5. Note from Fig. 5 that numerical and experimental values are in close agreement up to a settlement of 40 mm. However, the numerical method analysis gives less conservative load values than experimental load results with increasing settlement. The variations between the experimental and numerical results were found to be 13% and 17% for CPCC and UPCC, respectively. This variation between the results may be attributed to the fact that both CPCC and UPCC are treated as embedded columns while modeling in Plaxis 3D. Therefore, the installation effects such as variation of in-situ stresses due to installation disturbances during displacement installation of columns is not incorporated in the numerical modeling. Pervious concrete is modeled as linear elastic and pervious. The other parameters, such as column–soil interaction values, are limited due to the constraint of subroutine. This may be the reason that it yields fewer conservative results. The higher stiffness of the pervious concrete column without and with underreamed bulbs provides larger load-carrying capacity even in compressible soils (Golait and Padade 2018) and loose cohesionless soils such as pond ash, as in the present case.

An increased degree of consolidation and bearing capacity and reduced settlement were obtained for both CPCC and UPCC, however UPCC yielded more significant results. During the model testing and numerical modeling, the drainage property of both CPCC and UPCC was taken as constant throughout, which in reality varies with time due to clogging of the pores of PCC. Therefore, the future scope of the present work can include the effect of clogging of the voids in the pervious concrete columns and corresponding variation in the rate of consolidation.

#### Failure Mechanism of CPCC and UPCC

Fig. 6 presents the failure of the pervious concrete column without and with a single underreamed bulb. The failure of CPCC and UPCC has a marked feature of lateral deformation in the form of convex column shape on one side and concave shape on the other. The high stiffness of both CPCC and UPCC makes it independent of the confinement offered by the weak surrounding

pond ash (relative density of 40%). Due to stabilization of the surrounding soil having relative density of 40% using the traditional granular columns, the failure of columns by bulging at a depth of 1D to 3D ( $D =$  diameter of the column) was generally observed. This bulging is due to the insufficient lateral confinement offered by the poor surrounding soil. Conversely, pervious concrete columns possess high bond strength between the column materials due to the binder material. After curing, the pervious concrete columns gained the desired compressive strength and when subjected to vertical loading, underwent only punching failure in the case of floating columns. However, in the present case, both CPCC and UPCC are constructed as end-bearing columns and, hence, lateral convex and concave curving is observed under the compressive vertical loading and subsequent end bearing from the column bottom. During installation using the casing, the phenomenon of cavity expansion (soil moving downward and laterally outward) increases the vertical stress and, consequently, increases the interface friction at the column–soil interface. Furthermore, cavity expansion also leads to nonuniform lateral soil movement along the column length (Suleiman et al. 2014), which governs the column deformation during failure. Moreover, the deformation of columns as shown in Fig. 6 that appears like bulging is precisely a consequence of lateral movement of soil due to installation effect. During installation and subsequent retrieval of the casing, the surrounding soil is observed to be displaced laterally up to 1D distance from the column center. This lateral soil movement, however, diminishes beyond a depth of 5D (Suleiman et al. 2014). In the present study [Figs. 6(a and b)], the local deformation of columns is found to occur at about 4D. Moreover, lateral bulging is primarily associated with stone columns and encased stone columns only.

### Theoretical Analysis

Golait and Padade (2018) described the analytical and experimental work on cemented stone columns without and with underreaming bulbs located at the bottom and intermediate depth of  $5d$  ( $d =$  diameter of the column) from the top surface. However, the analytical solution was developed for compressible clay soil only. In the present study, an attempt is made to test the pervious concrete column with the circular cross section and underreamed bulb at  $2d$  distance from the top surface. The use of pervious concrete contributes to accelerating the consolidation process and utilizing its high stiffness for improving the weak surrounding cohesionless soil. The various forces acting along the CPCC and UPCC under vertical applied force [Figs. 7(a and b)] are described as:

1. The resistance offered by the unit-cell boundary soil area ( $A_u - a_s$ ) within the assumed local shear failure of loose to medium dense cohesionless soil underneath the rigid circular plate base ( $R_s$ ), where  $a_s =$  area of the stone column, and  $A_u =$  unit cell area.
2. The development of shaft skin friction resistance ( $R_f$ ) over the length of the column.
3. The mobilized resistance offered by the underreamed bulb ( $R_b$ )
4. The point tip resistance mobilized at the bottom of the column ( $R_t$ )

To balance the static vertical forces the following equation is used

$$Q_f = R_s + R_f + R_b + R_t \quad (1)$$

The different forces that act on the column which contributes to carrying the load involved in Eq. (1), can be formulated with the following assumptions:

1. The soil is loose to medium dense (relative density is less than 60%), the angle of shearing resistance  $\phi = 28^\circ$  (local shear failure), and cohesion is small (less than 1 kPa).

2. The skin-friction resistance (shaft) develops over the length of the column and tip resistance develops at bottom of the column ( $R_t = L/d$ ).
3. The enlarged area (underreaming bulb) assumed as horizontal, the resistance develops is  $R_b$ .
4. The bearing capacity factor is assumed to vary from zero (at  $2d$ ) to 1 (at  $22d$ ), where  $d =$  column diameter [Fig. 7(c)]. The reduction value of  $r_d$  at any depth  $z$  along the length of the column can be given as

$$r_d = 0.05 \left( \frac{z}{d} \right) - 0.1 \quad (2)$$

As per Terzaghi's bearing capacity analysis for strip footing, the failure of the footing takes place within the width of the footing. The bearing capacity starts to reduce beyond one width of the footing. From Boussinesq's theory of pressure bulb, the resistance offered by the pile reduces beyond two times the footing width. Moreover, as per the conventional pile foundation analysis, the resistance offered by the pile skin friction reduces beyond two to three times the pile diameter.

5. It is assumed that the top layer of loose to medium dense soil within  $2d$  depth participates in the local shear failure below the circular loading plate.

### Analysis of Unit Cell Concept for Underreamed Pervious Concrete Column (UPCC)

A rigid circular plate of diameter  $D_u$  placed on loose to medium cohesionless soil is assumed to develop local shear failure of depth equal to  $D_u$ . The ultimate bearing capacity (UBC) can be given as

$$\text{UBC} = \sigma' \cdot N_q \quad (3)$$

where  $\sigma' =$  Effective overburden pressure;  $\sigma' = \gamma L$ ; and  $N_q =$  bearing capacity factor.

$R_s =$  resistance offered by the area ( $A_p - a_s$ ), where  $A_p =$  area of the circular plate,  $a_s =$  area of the column.  $R_s$  can therefore be expressed as

$$R_s = \sigma' \cdot N_q \cdot (A_p - a_s) \quad (4)$$

Simplifying Eq. (4) by substituting the  $A_p$  and  $a_s$  values and introducing a nondimensional parameter ( $R_a$ ) for area replacement ratio defined as  $R_a = a_s/A_p$ , Eq. (4) can be written as

$$R_s = \sigma' \cdot N_q \cdot A_p \left( 1 - \frac{a_s}{A_p} \right)$$

$$R_s = \sigma' \cdot N_q \cdot A_p \cdot (1 - R_a) \quad (5)$$

$R_f =$  ultimate skin friction resistance developed along the column surface over the length  $L_e$ .

$$L_e = [L - (Br - 1) \cdot d], \text{ where } L < L_e$$

The shaft resistance offered in loose cohesion less soil can be expressed as

$$Q_f = f_s \cdot (Ac)$$

$$f_s = (K \cdot \tan \delta \cdot \sigma_{\text{avg}})$$

$$R_f = (K \cdot \tan \delta \cdot \sigma_{\text{avg}}) \cdot \pi \cdot d \cdot L_e \quad (6)$$

where  $f_s =$  skin friction resistance;  $A_c =$  surface area of the column;  $K =$  lateral earth pressure coefficient;  $\sigma_{\text{avg}} =$  average effective overburden pressure; and  $\tan \delta =$  coefficient of friction between soil and pile.

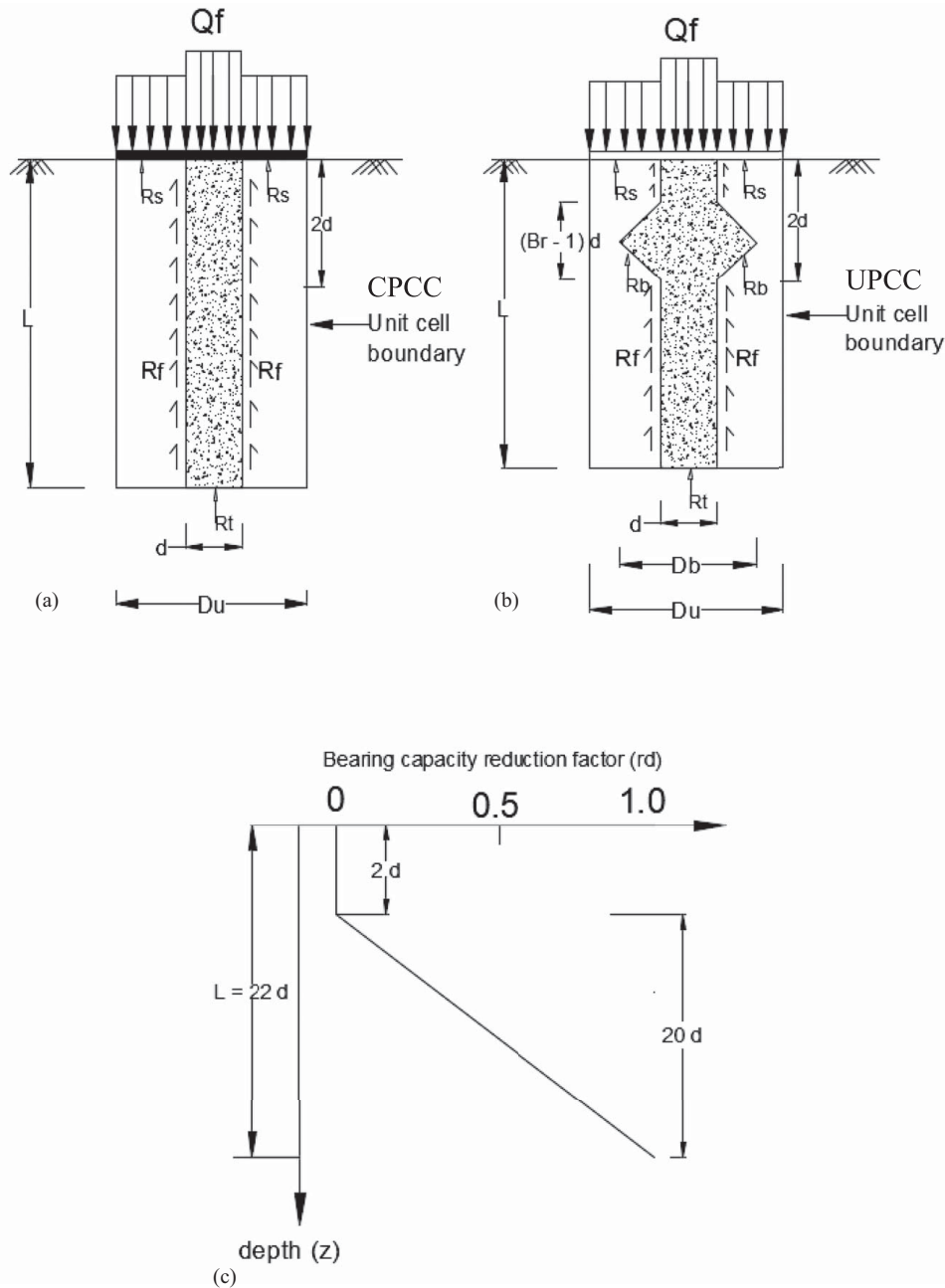


**Fig. 7.** Free-body diagram and forces acting on columns made up of pervious concrete of (a) circular section; (b) underreamed single bulb; and (c) reduction of bearing capacity with the depth.

By simplifying Eq. (6) and using

$$L_e = [L - (Br - 1) \times d]$$

where  $B_r$  = bulb ratio =  $d^2/D_b^2$ ; and  $K$  = lateral earth pressure coefficient, recommended as 0.5 for loose cohesionless soil,  $R_f$  can be given as

$$R_f = 1.57(\sigma' \cdot \tan \delta) \cdot [L \cdot d - (Br - 1) \cdot d^2] \quad (7)$$

The third component of the column is the resistance offered by the bulb,  $R_b$  (for a column with single bulb) and  $R_b = 0$  for a uniform cross section of the column. The resistance is offered by the horizontal projected part of the bulb, calculated as  $A_b - a_s$ , where  $A_b$  = horizontal projected bulb area. The resistance mobilized at this zone is less than the ultimate resistance at the tip of the column. The reduction of the resistance is determined in terms of the

bearing capacity reduction factor ( $R_{bd}$ ) from the location of the bulb at length  $(L - 2d)$ . Eq. (2) can thus be modified as

$$R_{bd} = 0.05 \cdot \left( \frac{L - 2d}{d} \right) - 0.1$$

$$R_{bd} = 0.05(R_L - 2) - 0.1 \quad (8)$$

where  $R_L$  = length ratio given by  $R_L = L/d$ .

Thus, bulb resistance  $R_b$  can be calculated as

$$R_b = \sigma' \cdot N_q \cdot (A_b - a_s) \cdot (1 - R_{bd})$$

where

$$(A_b - a_s) = 0.785(B_r^2 - 1) \times d^2$$

$$R_b = (1.2 - 0.05R_L) \cdot [0.785 \cdot d^2(B_r^2 - 1)] \cdot \sigma' \cdot N_q \quad (9)$$

The tip resistance  $R_t$  is offered at the bottom of the column and depends on the bearing capacity reduction factor at the column tip. Referring to Eq. (2), the bearing reduction can be written as

$$R_{bd} = 0.05 \left( \frac{L}{d} \right) - 0.1$$

Hence,

$$R_t = \sigma' \cdot N_q \cdot a_s (1 - R_{bd})$$

Simplifying this equation by substitution of the reduction factor value  $R_{bd}$  gives

$$R_t = (1.2 - 0.05R_L)(0.785d^2) \cdot \sigma' \cdot N_q \quad (10)$$

where  $\sigma'$  = effective overburden pressure at the tip of the column; ( $\sigma' = \gamma \cdot L$ ); and  $N_q$  = bearing capacity factor.

The load-carrying capacity at the failure  $(q_f)_u$  for reinforced loose cohesionless soil can thus be determined as

$$(q_f)_u = \frac{Q}{A} = \left[ \frac{R_s}{A} + \frac{R_f}{A} + \frac{R_b}{A} + \frac{R_t}{A} \right]$$

$$\frac{R_s}{A} = \sigma' \cdot N_q \cdot \frac{A_p}{A} \cdot (1 - R_a)$$

$$\frac{R_s}{A} = \sigma' \cdot N_q \cdot (1 - R_a) \quad (11)$$

From Eq. (5),

$$\frac{R_f}{A} = 1.57(\sigma' \cdot \tan \delta) \cdot \left[ L \cdot \frac{d}{A} - (B_r - 1) \cdot \frac{d^2}{A} \right]$$

where

$$L \cdot \frac{d}{A} = L \cdot \frac{4}{\pi} \cdot \frac{d}{D_u^2}$$

$$L/d = R_L, \text{ and } d^2/D_u^2 = R_a$$

Further substituting and simplifying Eq. (5), the following is obtained:

$$\frac{R_f}{A} = 2(\sigma' \cdot \tan \delta) \cdot R_a \cdot [R_L - B_r + 1] \quad (12)$$

From Eq. (9),

$$\frac{R_b}{A} = (1.2 - 0.05R_L) \cdot \left[ 0.785 \cdot \frac{d^2}{A} (B_r^2 - 1) \right] \cdot \sigma' \cdot N_q$$

$$\frac{R_b}{A} = (1.2 - 0.05R_L) \cdot [R_a \cdot (B_r^2 - 1)] \cdot \sigma' \cdot N_q \quad (13)$$

From Eq. (10),

$$\frac{R_t}{A} = (1.2 - 0.05R_L) \left( 0.785 \frac{d^2}{A} \right) \cdot \sigma' \cdot N_q$$

$$\frac{R_t}{A} = (1.2 - 0.05R_L)(R_a) \cdot \sigma' \cdot N_q \quad (14)$$

Therefore, by adding Eqs. (11)–(14), the ultimate failure load-carrying capacity  $(q_f)_u$  of reinforced loose cohesionless soil for the underreamed bulb can be determined as

$$(q_f)_u = \sigma' \cdot N_q(1 - R_a) + 2\sigma' \cdot \tan \delta \cdot R_a[R_L - B_r + 1]$$

$$+ (1.2 - 0.05R_L) \cdot R_a \cdot (B_r^2 - 1) \cdot \sigma' N_q$$

$$+ (1.2 - 0.05R_L) \cdot R_a \cdot \sigma' N_q \quad (15)$$

### Analysis of CPCC without Underreamed Bulb

Fig. 7(a) shows the forces acting on a uniform circular cross section pervious concrete column under the applied force  $Q_f$  and the mobilized resisting forces acting along the column as  $R_s$ ,  $R_f$ , and  $R_t$ . The resisting forces are constant due to the uniform circular cross section. Since there is no underreamed bulb, the resistance mobilized due to the enlarged projected bulb ( $R_b$ ) is considered as zero. Hence, Eq. (15) is simplified and rewritten as

$$(q_f)_c = \sigma' \cdot N_q(1 - R_a) + 2\sigma' \cdot \tan \delta \cdot R_a[R_L - B_r + 1]$$

$$+ (1.2 - 0.05R_L) \cdot R_a \cdot \sigma' N_q \quad (16)$$

Considering the circular rigid base plate of diameter  $D_u$  and area  $A$ , resting on the loose to medium-dense cohesionless soil, the ultimate bearing capacity  $q_f$  is expressed as

$$q_f = \sigma' \cdot N_q \quad (17)$$

### Load-Carrying Capacity Improvement Factor

The amount of ultimate bearing capacity of loose to medium-dense cohesionless soil can be increased by installation of pervious concrete columns. The load-carrying capacity improvement factor (LCF) is defined as the ratio of ultimate load carried by the column reinforced composite ground to the ultimate load carried by the unreinforced ground. The equation of LCF for reinforced loose to medium-dense cohesionless soil by a UPCC can be obtained by dividing Eq. (15) by Eq. (17). Similarly, dividing Eq. (16) by Eq. (17) gives the LCF for CPCC. The calculation values are in agreement with IS 2911 (Part 1/sec 2) used for bored cast in-situ concrete piles. The LCF value depends on three nondimensional parameters characterizing the replacement ratio ( $R_a$ ), column-length ratio ( $R_L$ ), and underreaming ratio ( $B_r$ ).

The load values at the 7-mm settlement measured from the experimental results and computed with the help of the developed equations are detailed in Table 3. Not from Table 3 that the measured and computed values are in good agreement, within permissible error range of 4.4%.

The load-carrying improvement factor was calculated by varying the area replacement ratio ( $R_a = 12.3\%$ ,  $16\%$ ,  $20\%$ ) and column-length ratio ( $R_L = 5, 7, 10, 15, 20$ ). The bulb ratio ( $B_r$ ) was kept constant at 2.5 (BIS 2010 (Part 1/sec 2)). It is evident from Fig. 8(a) that the load-carrying improvement factor for UPCC increases with increase in the area replacement ratio ( $R_a$ )

**Table 3.** Validation of analytical results with experimental results

S. No.	Description	Experiment (kPa)	Analytical (kPa)	Settlement (mm)	Error (%)
1	Underreamed bulb with pervious concrete	133	132	7	0.75
2	Circular section with pervious concrete	113.7	108.9	7	4.4

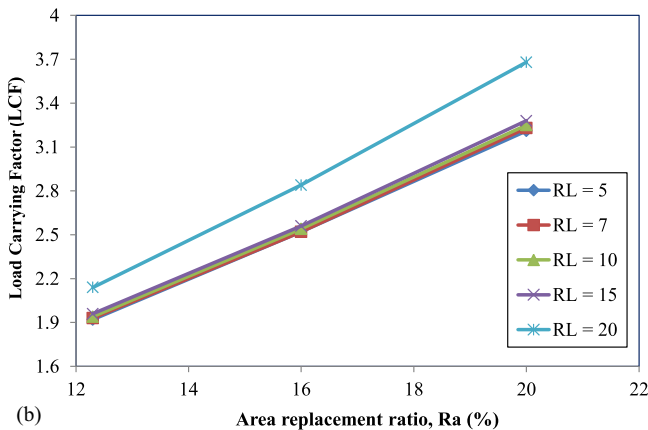
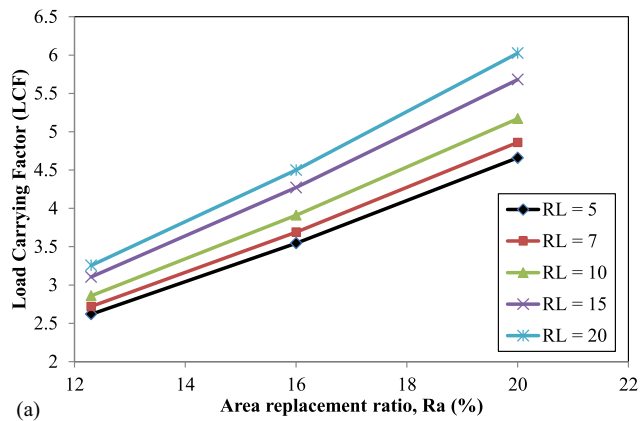


**Fig. 8.** Variation of LCF with area replacement ratio at  $B_r = 2.5$  for (a) UPCC; and (b) CPCC from theoretical analysis.

and column-length ratio ( $R_L$ ). The LCF is found to increase up to 6.02 for  $R_a = 20\%$  and  $R_L = 20$  at a bulb ratio of 2.5.

In the case of CPCCs, as shown in Fig. 8(b), the trend line of the increment is almost identical to UPCC, with slight variation up to  $R_a = 20\%$ , and as the  $R_L$  is increased up to 15%. At  $R_L = 20$ , LCF value increases with the area replacement ratio. At the  $R_a = 20\%$  and  $R_L = 20$ , the LCF is 64% more in UPCC than in the CPCC. This is due to the enlarged area of the bulb, which contributes to its effectiveness in bearing the axially applied load in loose cohesionless soil.

The variation of LCF with changing bulb ratio ( $B_r$ ) from 2, 2.5, and 3 is shown in Fig. 9. It is observed that as  $R_a$  increase from 12% to 20%, an increment rate of 25% is observed constantly for LCF. As for IS 2911 (part III: 2006), for a bulb ratio of 2.5, LCF value of 2.72 is obtained with an area replacement ratio of 12.3%, which is in accordance to the obtained values. Also, a close agreement is found between the calculated values and published data by Golait and Padade (2018) for cemented stone columns.

### Consolidation Studies Using 3D Numerical Model

To understand the efficacy of the pervious concrete column, consolidation analysis is conducted on an embankment model on untreated pond ash and on pond ash fill supported with pervious concrete columns. The case study aims to record the time rate of expulsion of excess pore water pressure and amount of time

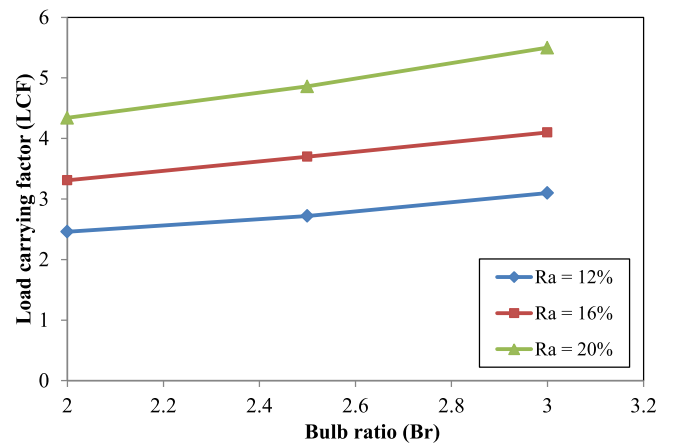


**Fig. 9.** Variation of LCF with  $B_r = 2, 2.5, 3$  and area replacement ratio from theoretical analysis.

allowed to achieve the maximum degree of consolidation for treated pond ash fill using the Plaxis 3D [finite-element analysis (FEA)].

### Parametric Study

The embankment is constructed to a total height of 4 m in two stages. In the first stage, 2 m height is constructed, which is then allowed to consolidate, and then another 2 m is constructed, which is further allowed to consolidate to a minimum excess pore water pressure. To make the analysis less cumbersome, only one-half of the embankment is analyzed, as shown in Fig. 10. The materials properties used for modeling the embankment, CPCC, and surrounding pond ash are summarized in Table 4. The numerical study has been carried out to check the efficacy of the PCCs with respect to dissipation of excess pore water pressure and change in the degree of consolidation when installed in pond ash subjected to embankment loading. The comparable study of CPCC and UPCC using numerical study has not been carried out to assess the dissipation and consolidation rate, since it is predominantly dependent on the behavior of the pervious concrete used. The comparable study depicting the effect of bulb as in UPCC as compared with CPCC is best evaluated based on the experimental load–settlement investigation. The numerical study only denotes the drainage potential of the proposed columns which make them comparable with the free draining traditional stone columns.

### Modeling in Plaxis 3D

The consolidation analysis of the embankment on the pervious concrete column was carried out only for the static condition. The columns were treated as embedded columns in pond ash fill resting over a layer of sand (Fig. 10). The CPCC installed had a diameter of 1 m and were spaced at  $2.5d$  ( $d =$  diameter of the column). The embankment was constructed in two phases, with a 2-m lift in each phase. The pond ash was analyzed as soft soil and sand, and the embankment as hardening soil, while pervious concrete columns were modeled as a Mohr–Coulomb system. The material properties adopted for the various modeling elements were adopted as per the existing reported studies (Chandruppa and Biligiri 2016; Pul et al. 2017; Alkhorshid et al. 2021; Sudheer et al. 2021). The published  $k$  value (falling head test) equal to 0.01 m/s at the 10 kPa/m pressure was adopted based on Qin et al. (2015).

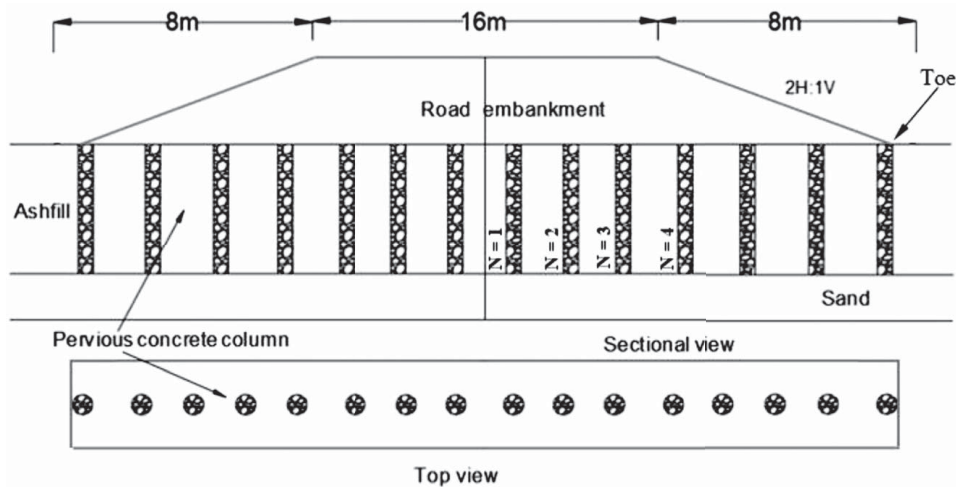


Fig. 10. Schematic representation of parametric study of road embankment (sketch not to the scale).

Table 4. Material properties used in the 3D numerical program

Material properties	Experimental values PA	Plaxis values for PA	Sand	Embankment	Experimental values PCC	Pervious concrete column
Model	Lab	Soft soil (SS)	Hardening soil (HS)	Hardening soil (HS)	Lab	Mohr-Columb (MC)
Bulk unit weight, $\gamma_{\text{unsat}}$ (kN/m <sup>3</sup> )	10	10	17	16	18	18
Saturated unit weight, $\gamma_{\text{sat}}$	12	12	20	19	19	19
Cohesion, $c'$ (kN/m <sup>2</sup> )	0.33	0.1	0	29	1	1
Friction angle, $\phi'$	28	28	33	30	32	32
Dilatancy angle, $\psi'$	0	0	3	0	2	2
Permeability "k" (m/s)	$0.86 \times 10^{-8}$	$0.8 \times 10^{-8}$	0.74	—	$7.14 \times 10^{-3}$	$7 \times 10^{-3}$

Sources: Data from Alkhorshid et al. (2021); Sudheer et al. (2021); Chandrappa and Biligiri (2016); Pul et al. (2017).

### Consolidation Analysis

Since consolidation progresses by the dissipation of excess pore water pressure, the degree of consolidation at any time is given by

$$U = \frac{U_o - U_t}{U_o} = 1 - \frac{U_t}{U_o} \quad (18)$$

where  $U$  = degree of consolidation;  $U_o$  = initial excess pore water pressure; and  $U_t$  = excess pore pressure at any time  $t_o$ .

### Case 1. Embankment on Pond Ash without Pervious Concrete Column

The embankment was constructed in two stages. When the first 2-m-high embankment was constructed, complete consolidation of soil was allowed prior to the modeling of then next 2-m-high embankment lift. The consolidation of the final 2 m was thereby allowed to consolidate. In this manner, the total consolidation occurred in two stages. In the first stage of loading, the excess pore pressure increases linearly up to 21.2 kN/m<sup>2</sup>. During the consolidation time, the excess pore water pressure dissipated in 27 days. In the second stage of loading, the excess pore pressure generated increased linearly to 27.94 kN/m<sup>2</sup> and took 79 days for complete dissipation. The total time for consolidation without any provision of drainage path (pervious concrete column) for a 4-m height loading embankment was therefore 79 days (Fig. 11).

### Case 2. Embankment Supports Soil with Pervious Concrete Column

To understand the contribution of CPCCs in improving the consolidation rate, a different number of CPCC ( $N=1, 2, 3,$  and  $4$ ) were installed at the middle of the embankment. However, for practical

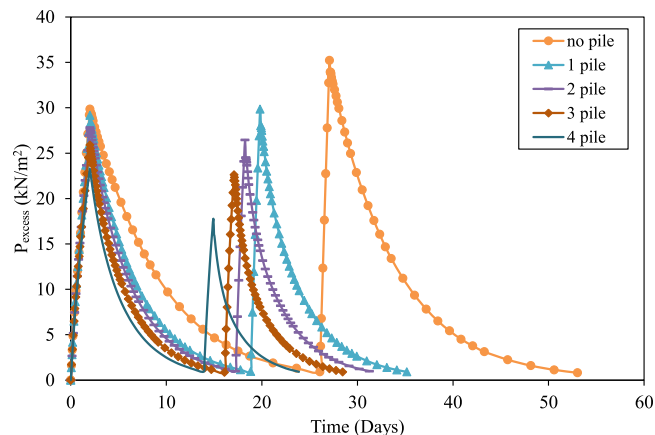
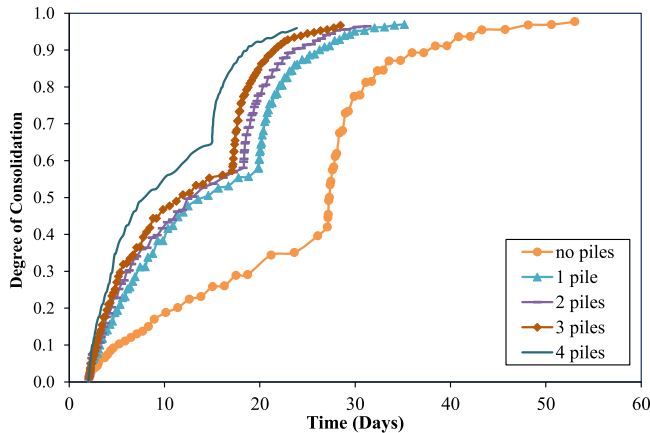


Fig. 11. Variation of excess pore water dissipation with different number of CPCC.

purposes, smaller spacing of columns beneath the central portion of the embankment as compared with the connecting side slope was reported to contribute more to reducing both the total and differential settlement than the columns under the sloping side of the embankment (El Kamash et al. 2014). Hence, use of four columns for assessing the bearing capacity improvement of pond ash beneath the critical central embankment portion signified the partial practicality of the used numerical model. However, previous studies (Rajagopal and Mohapatra 2016; Chai et al. 2017) reported that columns located near the toe of the embankment are subjected to lateral loading rather than vertical loading, which is acting on the columns near the center of the embankment. Based on this loading

scenario and for validation of model testing results available for vertical loading only, columns were placed beneath the center of the embankment. However, for practical purposes, the columns should be placed throughout the embankment base to counter the slip surface that induces the lateral load in the outer columns placed near the embankment toe. Therefore, the complete investigation of the practical scenario as shown in Fig. 10 was also carried out by using circular PCCs installed up to the toe of the embankment.

The embankment and its consolidation were simulated in two phases, similar to the previous case of untreated embankment. The provision of the pervious concrete column offered additional drainage path for better dissipation of the developed excess pore water pressure. It was observed that using one CPCC, the



**Fig. 12.** Variation of degree of consolidation with different number of CPCC.

maximum excess pore pressure developed was  $27.9 \text{ kN/m}^2$ , which takes about 39 days for dissipation. Similarly, with the CPCCs, the excess pore water pressure generated was found to be  $24 \text{ kN/m}^2$ . The total time for dissipation was recorded as 25 days for CPCCs. It was also observed that higher excess pore water pressures were developed during the second stage of loading (2-m embankment lift).

The decrease in the total excess pore water pressure dissipation time with increase in the number of the pervious concrete columns is attributed to the availability of additional drainage path in conjunction to the low permeable pond ash below the embankment. This also signifies that pervious concrete columns will be more suitable in clayey soils. However, the particle size of pond ash is classified as silt with coefficient of permeability ( $k$ ) in range of  $10^{-4}$  to  $10^{-6} \text{ m/s}$  (Kumar 2004; Bera et al. 2007; Havanagi et al. 2011; Mishra and Das 2012; Mohanty and Patra 2015). Furthermore, the Mishra and Das (2012) consolidation study on pond ash shows that the void ratio of the samples under incremental load applied of  $3.2 \text{ kg/cm}^2$  at 7 days was 0.908. Under similar loading, the void ratio decreased to 0.842 on the 35th day. Consequently, a delayed rate of consolidation was observed. However, numerical studies have also shown that the pervious concrete columns under the embankment load are found to give less significant results in context to drainage enhancement when compared with ordinary and encased stone columns (Sudheer et al. 2021). The PCCs are primarily useful for bearing capacity improvement.

From Fig. 12, it can be seen that 90% degree of consolidation is reached in 80 days for an embankment without pervious columns. However, the same embankment when supported with CPCC beneath the embankment base, 90% degree of consolidation is reached in approximately 27 days (Fig. 12). The total consolidation time taken by CPCCs is rather higher than the ordinary and encased

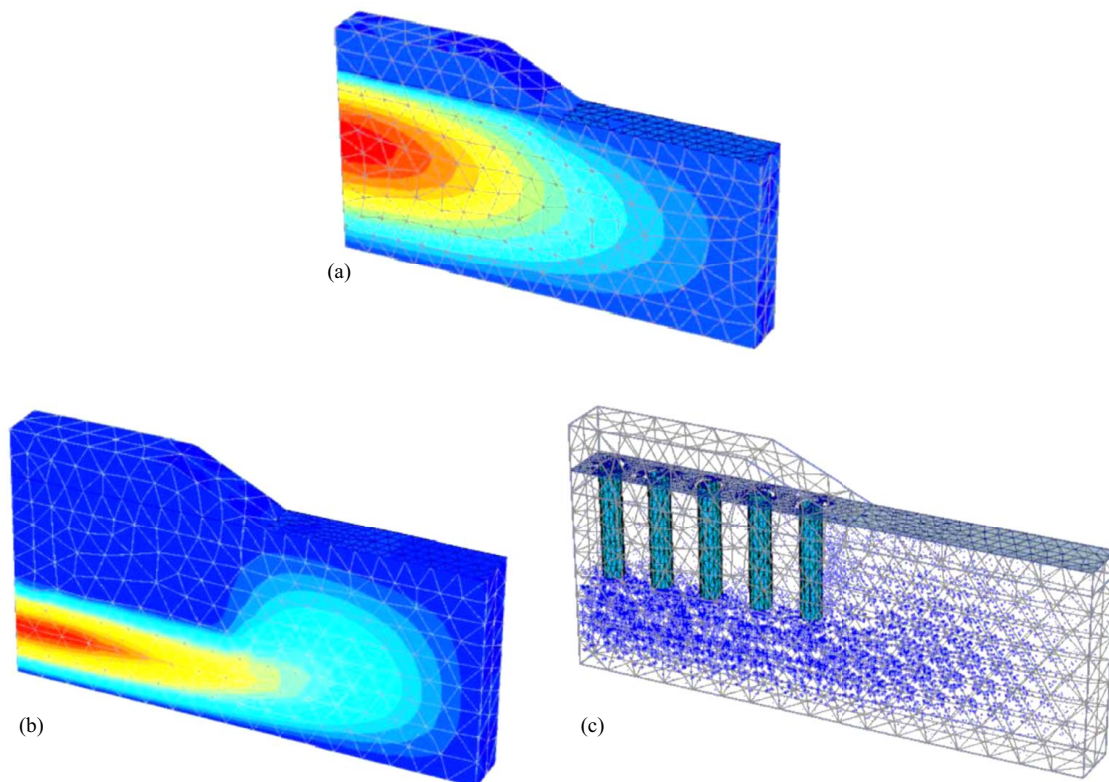


**Fig. 13.** Development of excess pore water pressure: (a) without CPCC; (b) with CPCC; and (c) flow path of excess pore water dissipation with CPCC beneath the embankment.

stone columns (Sudheer et al. 2021), which can be accounted for by the larger volume of interconnected voids present in granular columns. Furthermore, the void spaces within the CPCC columns may be interrupted by the cement gel formation due the reaction with water, leading to void clogging. It is evident from Fig. 13(a) that in absence of CPCCs, the excess pore water pressure generated dissipates through the ash pond layer spread beneath the embankment. The excess pore water pressure generated takes a much longer time to drain out because of the low permeability and distance equal to the thickness ash pond. Alternatively, with the provision of CPCCs, the drainage path is reduced. The generated excess pore water pressure follows the high drainage available due to CPCCs and thereby drains out through the underlying sand layer [Fig. 13(b)]. The drainage path created by the CPCCs, and the path taken up during dissipation of excess pore water pressure can be clearly seen in Fig. 13. Nevertheless, this quick dissipation leads to lowering of pore water pressure value beneath the embankment and consequently increasing the effective stress which in turn expedites the consolidation in comparison with the untreated pond ash.

However, for all practical scenarios, installation of columns up to the embankment toe provides higher excess pore water pressure dissipation than without columns. The maximum dissipation of  $28 \text{ kN/m}^2$  is obtained in about 38 days when CPCCs are provided up to the toe of the embankment. Without using columns, the maximum dissipation of excess pore water attained is only  $24.4 \text{ kN/m}^2$ , but it is attained in a smaller period of about 16.8 days [Fig. 14(a)]. It can also be seen from Fig. 14(b) that the degree of consolidation has reduced to half when using CPCC as compared with without columns. It is observed that 90% degree of consolidation is reached in 18 days with CPCCs when compared with 90% of degree of consolidation without column supported embankment, which takes 36 days. The development of excess pore water pressure is concentrated at the bottom of the embankment in the absence of columns. The developed excess pore water pressure is retained at the low permeability pond ash layer [Fig. 15(a)] but as the CPCCs are provided, additional drainage path is available for the excess pore water pressure to dissipate. The developed excess pore water pressure now moves away from the bottom of the embankment and takes up the path available in the free draining sand layers

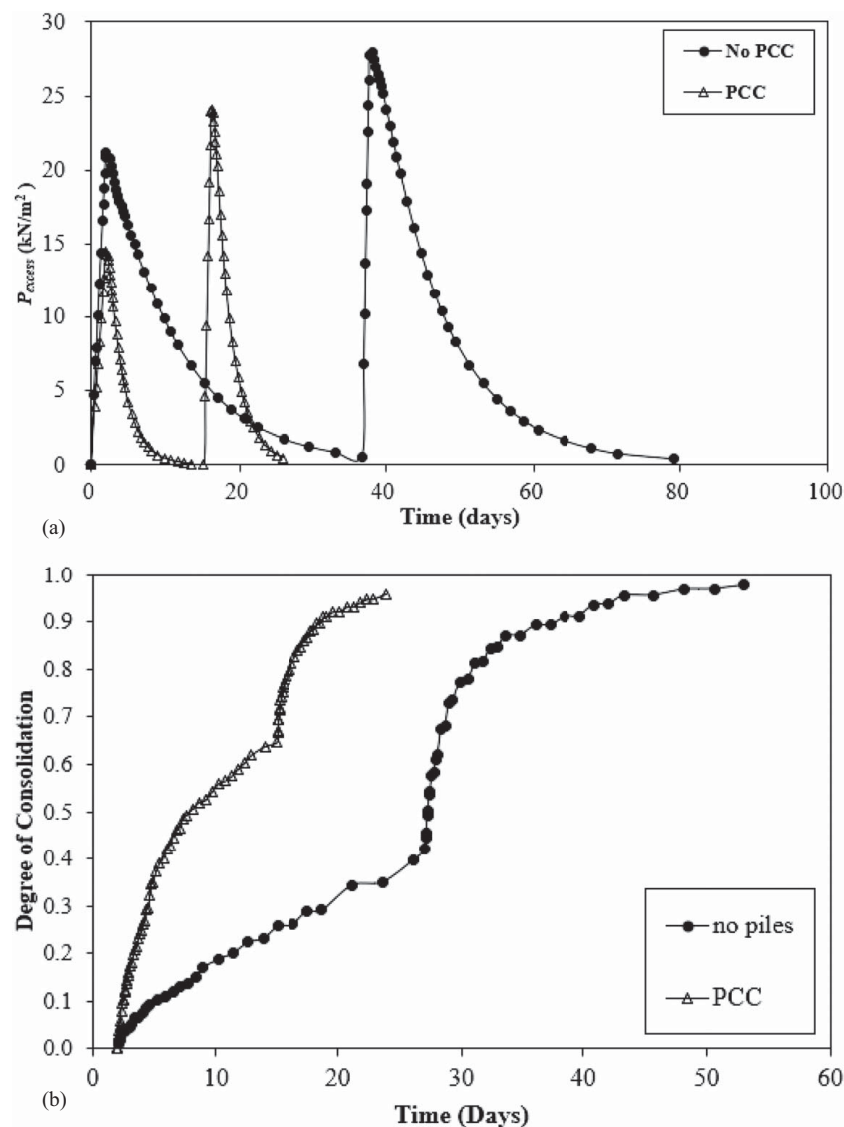


**Fig. 14.** (a) Variation of excess pore water dissipation without and with CPCCs provided up to the toe of the embankment; and (b) variation of degree of consolidation without and with CPCCs provided up to the toe of the embankment.

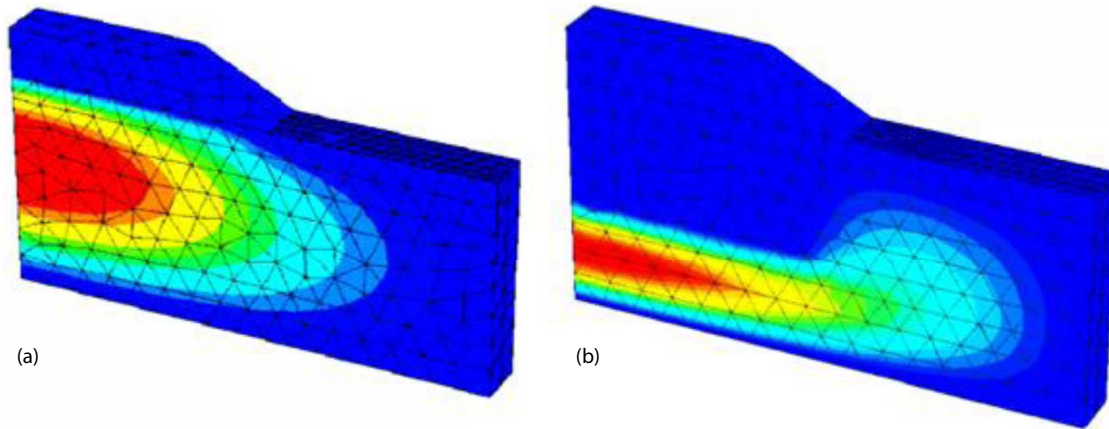


**Fig. 15.** Development of excess pore water pressure: (a) without CPCC; and (b) with CPCC provided up to the toe of the embankment.

[Fig. 15(b)]. This further signifies the advantage of CPCCs in expediting the dissipation of excess pore water pressure.

### Implementation of Proposed Methodology Using an Illustrative Example

The granular columns provide the drainage path, thereby increasing the time rate of consolidation, reducing the liquefaction potential, improving the bearing capacity, and reducing settlement. The ordinary columns have limited stiffness and the column failures due to bulging (at a depth equal to two times the diameter of the shaft) in soils with poor confinement. To overcome this limitation, stone columns are encased in geosynthetics, but this partially improves the failure mechanism. To address the drainage, low bearing capacity, excessive settlement, and very low undrained shear strength of compressible soil, the author(s) attempted to investigate columns having drainage of granular columns and stiffness of concrete columns, making it independent to the stiffness of the surrounding soil. Therefore, two types of columns, namely pervious concrete column without and with underreamed bulbs, are suggested. Based on the results, it is suggested that in case of fills with less-reactive elements, CPCCs can be easily installed using displacement-replacement method. Nevertheless, for attaining higher bearing capacity, field engineers can opt for PCC with a bulb at a depth of  $2D$  from ground level. However, the construction cost may add up due to the requirement of special underreaming tool for bulb formation. The practical application of CPCC and UPCC are strictly based on the prime requirement of the site. For project involving significant bearing capacity improvement over increased drainage, CPCC and UPCC are highly recommended. For site conditions with poor drainage but moderate lateral confinement, encased stone columns are suggested.

The following example site problem of the design of CPCC / UPCC layout for improvement of the loose cohesion-less soil ground is solved to highlight the application of the methodology described in the paper.

A thermal power station to install the steam turbines at the base the mat foundation of 9 m in diameter is constructed on a site of very old ash fill dump site the deep deposit 12 m thick and underlain by a rocky stratum and water table is at 8 m from the surface. The proposed structure design foundation pressure is 130 kPa. The geotechnical tests were conducted in laboratory, from the direct shear test the shear strength parameters of soil obtained as, cohesion  $c_d = 0$ , angle of friction  $= 30^\circ$ . For the proposed pervious concrete column,  $E_c = 15,000$  kPa.

The purpose is to design an appropriate layout of pervious concrete columns for a factor of safety of 2–2.5 for the bearing capacity and estimate the settlement of the structure.

### Solution

The pervious concrete column of 0.4 m in diameter ( $d_s$ ), spacing between center to center is 1.25 m in an equilateral triangular pattern are proposed. The length of these columns ( $L$ ) is designed to as 8 m. Hence,  $D_u = 1.05 \times s = 1.05 \times 1.25 = 1.31$  m.

Area replacement ration,  $R_a = 0.785 (d_s \times d_s/s) = 0.785 (0.4 \times 0.4/1.25) = 0.1007$  (10%).

Column length ratio,  $R_L = L/d_s = 8/0.4 = 20$ .

Using Eq. (17), the ultimate bearing capacity of untreated ground with considering the water table effect = 120 kPa.

### UPCC

Using Eq. (15), the ultimate bearing capacity of UPCC treated ground is = 411.66 kPa.

Hence, with a small area replacement ratio of 10%, the bearing capacity improvement factor  $F_b$  is  $F_b = 411.66/120 = 3.43$ .

### CPCC

Using Eq. (16), the ultimate bearing capacity of CPCC treated ground is = 285.66 kPa.

Hence, with a small area replacement ratio of 10%, the bearing capacity improvement factor  $F_b$  is  $F_b = 285.66/120 = 2.38$ .

The factor of safety for the bearing capacity of UPCC treated ground to a proposed structure =  $411.66/140 = 2.94$  (OK).

The factor of safety for the bearing capacity of UPCC treated ground to a proposed structure =  $285.66/140 = 2.1$  (OK).

### Settlement Calculations

$$S_i = \frac{q \cdot B (1 - \mu^2)}{E_c} \cdot I$$

Untreated ground settlement = 310.61 mm ( $q = 130$ ,  $b = 9$  m,  $u = 0.25$ ,  $E = 3,000$ ,  $I = 0.86$ ).

Treated ground settlement = 68 mm ( $q = 130$ ,  $b = 9$  m,  $u = 0.15$ ,  $E = 15,000$ ,  $I = 0.86$ ).

### Conclusions

The following conclusions are drawn from the present study of experimental work on pervious concrete columns in circular (CPCC) and underreamed (UPCC) configurations.

1. Based on the experimental results, it can be concluded that load-carrying capacity and load-improvement ratios of UPCC is

greater than CPCC at equal settlement and equal area replacement ratio.

2. The total vertical displacement of pond ash fill treated with UPCC was reduced by 60% in comparison with CPCC. However, construction difficulties, such as caving-in of underreamed bulb walls, contribute to a disadvantage of UPCC.
3. For end-bearing CPCC and UPCC, the failure is characterized by lateral column deformation occurring at a distance of 4D from the ground owing the nonuniform lateral soil movement governed by the cavity expansion developed during displacement installation. This nonuniform lateral soil movement is negligible beyond 5D.
4. The load-carrying capacity is computed with the developed analytical equations for loose cohesionless soils reinforced with PCC without and with enlarged underreamed bulbs, and the computed results are in close agreement with the measured values.
5. At similar area replacement ratio, column-length ratio, and bulb ratio of 2.5, UPCC yields higher LCF (LCF = 6) value than CPCC (LCF = 3). For UPCC, LCF increases with increase in bulb ratio and area replacement ratio.
6. The consolidation studies depicted a reduction of 36% in the development of excess pore water pressure and 56% decrease in consolidation time beneath an embankment constructed on pond ash fill supported with four CPCCs at the middle of the embankment base. However, the time for consolidation with CPCC is still found to be greater than as reported with stone columns/encased stone columns. Therefore, it can be concluded that CPCCs are preferable for scenarios involving primarily bearing-capacity conditions than drainage concerns.
7. As per the practical scenario of using CPCCs throughout the bottom of the embankment up to the toe, greater dissipation of excess pore water pressure and lesser time (18 days) in attaining 90% degree of consolidation is obtained against a scenario with no columns under the embankment. Thus, it can be concluded that CPCCs significantly enhance the rate of consolidation of low permeability soils, such as pond ash.

### Scope of the Future Work

During the study, the permeability behavior of pervious concrete columns in loose cohesionless soils under axial loading was considered as constant. However, due to the solids present in ground water and also due to the internal chemical reactions occurring within the pervious concrete, clogging of pores becomes inevitable. Therefore, long-term drainage potential of pervious concrete columns must be investigated. Furthermore, the present study considered only the static loading condition; hence, behavior of PCCs under lateral and dynamic loading conditions to assess the efficacy against liquefaction of partially and fully saturated fine-grained soils must still be addressed. Slope stability analysis can also be verified with the PCC while changing the slope angle, orientation of PCC, and spacing. PCC is uneconomical when compared with stone columns at higher replacement ratios, hence modification in the construction methodology or design consideration must be examined to make it cost effective.

### Data Availability Statement

All data, models, or code that support the findings of this study are available from the corresponding author upon reasonable request.

### Acknowledgments

The authors are grateful to the principal of the DAV Institute of Engineering and Technology for granting the permission to work in the Civil Engineering laboratory. The authors also acknowledge the manual help received from the lab technicians during the model tank testing. The authors are also thankful to the reviewers for the suggestions, modifications, and corrections that have improved the overall manuscript.

### Notation

The following symbols are used in this paper:

- $A$  = area of the column;
- $A_b$  = area of the underreamed bulb;
- $A_c$  = surface area of the column;
- $A_p$  = area of the circular plate;
- $A_u$  = unit cell area;
- $a_s$  = area of the stone column;
- $B_r$  = underreamed bulb ratio;
- $D$  = diameter of the column;
- $D_b$  = underreamed bulb ratio;
- $D_u$  = circular plate diameter;
- $f_s$  = skin friction resistance;
- $K$  = coefficient of permeability;
- $K$  = lateral earth pressure coefficient;
- $L$  = length of the pervious concrete column;
- $L/D$  = length to diameter ratio of stone column;
- $L_e$  = effective length;
- $N_q$  = bearing capacity factor;
- $Q_f$  = total applied load;
- $q_f$  = ultimate load-carrying capacity at failure of untreated soil;
- $(q_f)_u$  = ultimate load-carrying capacity at failure of treated soil;
- $R_a$  = area replacement ratio;
- $R_b$  = resistance force offered by the bulb;
- $R_{bd}$  = bearing capacity reduction factor;
- $R_D$  = relative density;
- $R_f$  = skin friction force;
- $R_L$  = length ratio of the column;
- $R_s$  = resistance force offered from soil below the circular plate;
- $R_t$  = tip resistance force of the column;
- $r_d$  = reduction factor;
- $S/D_c$  = settlement ratio (total settlement to diameter of concrete column);
- $U$  = degree of consolidation;
- $U_0$  = initial excess pore water pressure;
- $U_t$  = excess pore water pressure at any time  $t_0$ ;
- $Z$  = depth of the soil;
- $\delta$  = friction between soil and pile (interface);
- $\phi$  = angle of internal friction;
- $\gamma$  = unit weight of soil;
- $\sigma'$  = effective overburden pressure; and
- $\sigma_{avg}$  = average effective overburden pressure.

### References

- Alexiew, D., and M. Raithel. 2015. "Geotextile-encased columns: Case studies over twenty years." In *Ground improvement case histories*, edited by E. B. Indraratna, J. Chu, and C. Rujikiatkamjorn, 451–477. Oxford, UK: Elsevier.
- Alkhorshid, N. R., G. L. S. Araujo, and E. M. Palmeira. 2021. "Consolidation of soft clay foundation improved by

- geosynthetic-reinforced granular columns: Numerical evaluation." *J. Rock Mech. Geotech. Eng.* 13 (5): 1173–1181. <https://doi.org/10.1016/j.jrmge.2021.03.004>.
- Ali K., J. T. Shahu, and K. G. Sharma. 2014. "Model tests on single and groups of stone columns with different geosynthetic reinforcement arrangement." *Geosynth. Int.* 2 (2): 103118. <https://doi.org/10.1680/gein.14.00002>.
- Andhra Pradesh Power Generation Corporation Ltd. 2019. *Environmental appraisal report to use domestic washed coal in place of imported coal*. Vijayawada, India: Andhra Pradesh Power Generation Corporation Ltd.
- Barksdale, R. D., and R. C. Bachus. 1983. *Design and construction of stone columns*. FHWA/RD 83/026, Rep. No. 1, Vol. 1. Washington, DC: Federal Highway Administration.
- Bera, A. K., A. Ghosh, and A. Ghosh. 2007. "Compaction characteristics of pond ash." *J. Mater. Civ. Eng.* 19 (4): 349. [https://doi.org/10.1061/\(ASCE\)0899-1561\(2007\)19:4\(349\)](https://doi.org/10.1061/(ASCE)0899-1561(2007)19:4(349)).
- Bergado, D. T., J. C. Chai, M. C. Alfaro, and A. S. Balasubramaniam. 1994. *Improvement techniques of soft ground in subsiding and lowland environment*. Rotterdam, Netherlands: Balkema.
- Bhatt, A., S. Priyadarshini, A. A. Mohanakrishnan, A. Abri, M. Sattler, and S. Techapaphawit. 2019. "Physical, chemical, and geotechnical properties of coal fly ash: A global review." *Case Stud. Constr. Mater.* 11: e00263. <https://doi.org/10.1016/j.cscm.2019.e00263>.
- BIS (Bureau of Indian Standard). 2010. *(Part 1/sec 2), design and construction of pile foundations—code of practice, bored cast in-situ concrete piles*. IS 2911:1.2. New Delhi, India: BIS.
- Cai, J., G. Du, H. Xia, and C. Sun. 2021. "Model test and numerical simulation study on bearing characteristics of pervious concrete pile composite foundation." *KSCE J. Civ. Eng.* 25 (10): 3679–3690. <https://doi.org/10.1007/s12205-021-1522-7>.
- CBMP (China Building Materials Press). 2018. *Technical code for composite foundation of pervious concrete pile*, 9–10. DB37/T 5214-2018. Beijing: CBMP.
- Cengiz, C., and E. Güler. 2018. "Seismic behavior of geosynthetic encased columns and ordinary stone columns." *Geotext. Geomembr.* 46 (1): 40–51. <https://doi.org/10.1016/j.geotextmem.2017.10.001>.
- Chai, J.-c., S. Shrestha, T. Hino, and T. Uchikoshi. 2017. "Predicting bending failure of CDM columns under embankment loading." *Comput. Geotech.* 91: 169–178. <https://doi.org/10.1016/j.compgeo.2017.07.015>.
- Chandrupa, A. K., and K. P. Biligiri. 2016. "Pervious concrete as a sustainable pavement material – research findings and future prospects: A state-of-the-art review." *Constr. Build. Mater.* 111: 262–274. <https://doi.org/10.1016/j.conbuildmat.2016.02.054>.
- Chandrupa, A. K., and K. P. Biligiri. 2018. "Pore structure characterization of pervious concrete using X-ray micro-computed tomography." *J. Mater. Civ. Eng.* 30 (6): 04018108. [https://doi.org/10.1061/\(ASCE\)MT.1943-5533.0002285](https://doi.org/10.1061/(ASCE)MT.1943-5533.0002285).
- Chen, J.-F., L.-Y. Li, Z. Zhang, X. Zhang, C. Xu, S. Rajesh, and S.-Z. Feng. 2021. "Centrifuge modeling of geosynthetic-encased stone column-supported embankment over soft clay." *Geotext. Geomembr.* 49 (1): 210–221. <https://doi.org/10.1016/j.geotextmem.2020.10.021>.
- CRRI (Central Road Research Institute). 2019. *CSIR-CRRI annual report 2018-19*. Delhi, India: CRRI.
- El Kamash, W., J. Han, and F. Asce. 2014. "Displacements of column-supported embankments over soft clay after widening considering soil consolidation and column layout: Numerical analysis." *Soils Found.* 54 (6): 1054–1069. <https://doi.org/10.1016/j.sandf.2014.11.002>.
- Golait, Y. S., and A. H. Padade. 2017. "Analytical and experimental studies on cemented stone columns for soft clay ground improvement." *Int. J. Geomech.* 17 (4): 04016100. [https://doi.org/10.1061/\(ASCE\)GM.1943-5622.0000779](https://doi.org/10.1061/(ASCE)GM.1943-5622.0000779).
- Golait, Y. S., and A. H. Padade. 2018. "Enhancement in effectiveness of cemented stone columns for soft clay ground improvement by providing underreamed bulbs." *Int. J. Geomech.* 18 (11): 04018149. [https://doi.org/10.1061/\(ASCE\)GM.1943-5622.0001282](https://doi.org/10.1061/(ASCE)GM.1943-5622.0001282).
- Gupta, N., K. K. Yadav, and V. Kumar. 2015. "A review on current status of municipal solid waste management in India." *J. Environ. Sci.* 37 (1): 206–217. <https://doi.org/10.1016/j.jes.2015.01.034>.
- Harle, S. M. 2019. "Experimental investigation on the use of Pond Ash in the concrete." *Int. J. Sci. Res. Network Secur. Commun.* 7 (3): 12–20.
- Havanagi, V. G., A. K. Sinha, and S. Mathur. 2011. "Design and stability analysis of pond ash railway embankment." In *Geotechnical Engineering for Disaster Mitigation and Rehabilitation and Highway Engineering 2011: Geotechnical and Highway Engineering—Practical Applications, Challenges and Opportunities (With CD-ROM)*, 349–355.
- Hosseinpour, I., C. Soriano, and M. S. S. Almeida. 2019. "A comparative study for the performance of encased granular columns." *J. Rock Mech. Geotech. Eng.* 11 (2): 379–388. <https://doi.org/10.1016/j.jrmge.2018.12.002>.
- Hung, V. V., S.-Y. Seo, H.-W. Kim, and G.-C. Lee. 2021. "Permeability and strength of pervious concrete according to aggregate size and blocking material." *Sustainability* 13 (1): 426. <https://doi.org/10.3390/su13010426>.
- Khabbazian, M., V. N. Kaliakin, and C. L. Meehan. 2010. "Numerical study of the effect of geosynthetic encasement on the behavior of granular columns." *Geosynth. Int.* 17 (3): 132–143. <https://doi.org/10.1680/gein.2010.17.3.132>.
- Kim, S., D. Lee, J. Lee, S.-K. You, and H. Choi. 2012. "Application of recycled aggregate porous concrete pile (RAPP) to improve soft ground." *J. Mater. Cycles Waste Manage.* 14 (4): 360–370. <https://doi.org/10.1007/s10163-012-0076-7>.
- Kumar, S. J., S. Rawat, and A. K. Gupta. 2020. "Loose ash fills reinforced with the high confined encased stone columns: Experimental and numerical investigation." *Geotech. Geol. Eng.* 39: 2503–2520. <https://doi.org/https://doi.org/10.1007/s10706-020-01641-7>.
- Kumar, J. S., and P. Sharma. 2018. "Geotechnical properties of pond ash mixed with cement kiln dust and polypropylene fiber." *J. Mater. Civ. Eng.* 30 (8): 04018154. [https://doi.org/10.1061/\(ASCE\)MT.1943-5533.0002334](https://doi.org/10.1061/(ASCE)MT.1943-5533.0002334).
- Kumar, V. 2004. "Compaction and permeability study of pond ash amended with locally available soil and hardening agent." *J. Inst. Eng.* 85 (mai): 31–35.
- Lin, H., M. T. Suleiman, H. M. Jabbour, D. G. Brown, and E. Kavazanjian Jr. 2016. "Enhancing the axial compression response of pervious concrete ground improvement piles using biogrouting." *J. Geotech. Geoenviron. Eng.* 142 (10): 04016045. [https://doi.org/10.1061/\(ASCE\)GT.1943-5606.0001515](https://doi.org/10.1061/(ASCE)GT.1943-5606.0001515).
- Mishra, D. P., and S. K. Das. 2012. "One-dimensional consolidation of sedimented stowed pond ash." *Geotech. Geol. Eng.* 30 (4): 685–695. <https://doi.org/10.1007/s10706-011-9486-x>.
- Mohanty, S., and N. R. Patra. 2015. "Geotechnical characterization of Panki and Panipat pond ash in India." *Int. J. Geo-Eng.* 6 (1): 1–18. <https://doi.org/10.1186/s40703-015-0013-4>.
- Mohapatra, S. R., and K. Rajagopal. 2017. "Undrained stability analysis of embankments supported on geosynthetic encased granular columns." *Geosynth. Int.* 24 (5): 465–479. <https://doi.org/10.1680/jgein.17.00015>.
- Munaga, T., M. M. Khan, and K. K. Gonavaram. 2020. "Axial and lateral loading behavior of pervious concrete pile." *Indian Geotech. J.* 50 (3): 505–513. <https://doi.org/10.1007/s40098-019-00377-3>.
- Murugesan, S., and K. Rajagopal. 2006. "Geosynthetic-encased stone columns: Numerical evaluation." *Geotext. Geomembr.* 24 (6): 349–358. <https://doi.org/10.1016/j.geotextmem.2006.05.001>.
- Murugesan, S., and K. Rajagopal. 2010. "Studies on the behavior of single and group of geosynthetic encased stone columns." *J. Geotech. Geoenviron. Eng.* 136 (1): 129–139. [https://doi.org/10.1061/\(ASCE\)GT.1943-5606.0000187](https://doi.org/10.1061/(ASCE)GT.1943-5606.0000187).
- Ni, L., M. T. Suleiman, and A. Raich. 2016. "Behavior and soil–structure interaction of pervious concrete ground-improvement piles under lateral loading." *J. Geotech. Geoenviron. Eng.* 142 (2): 04015071. [https://doi.org/10.1061/\(ASCE\)GT.1943-5606.0001393](https://doi.org/10.1061/(ASCE)GT.1943-5606.0001393).
- Prakash, C., and V. Ramakrishna. 2004. "Lateral load capacity of underreamed piles—An analytical approach." *Soils Found.* 44 (5): 51–65. [https://doi.org/10.3208/sandf.44.5\\_51](https://doi.org/10.3208/sandf.44.5_51).
- Pul, S., A. Gaffari, E. Oztekin, M. Husem, and S. Demir. 2017. "Experimental determination of cohesion and internal friction angle on conventional concretes." *Mat. J.* 114 (3): 407–416.

- Qin, Y., H. Yang, Z. Deng, and J. He. 2015. "Water permeability of pervious concrete is dependent on the applied pressure and testing methods." *Adv. Mater. Sci. Eng.* 2015: 404136.
- Qing, J., C. Xin-Zhuang, C. She-Qiang, Z. Jiong, L. Feng, W. Xue-Zhi, and W. Yi-Lin. 2021. "In situ evaluation and analysis of improvement effects of pervious concrete pile on alluvial silt ground." *Geomech. Geoeng.* 16 (3): 212–222. <https://doi.org/10.1080/17486025.2019.1651404>.
- Rajagopal, K., and S. R. Mohapatra. 2016. "Behavior of geosynthetic encased granular columns under vertical and lateral loading." In *Proc., 6th Asian Regional Conf., on Geosynthetics - Geosynthetics for Infrastructure Development*.
- Rashma, R. S. V., R. Shivashankar, and B. R. Jayalekshmi. 2021. "Shear response of pervious concrete column improved ground." *Indian Geotech. J.* 51 (5): 1078–1086. <https://doi.org/10.1007/s40098-020-00473-9>.
- Sonawane, P. G., and A. K. Dwivedi. 2013. "Technical properties of pond ash-clay fired bricks—an experimental study." *Am. J. Eng. Res.* 2 (9): 110–117.
- Sudheer, K. J., S. Rawat, and A. K. Gupta. 2021. "Consolidation and bearing capacity studies on solid waste ash fill by using the hybrid granular piles." *Innovative Infrastruct. Solutions* 2022 (7): 76. <https://doi.org/10.1007/s41062-021-00664-0>.
- Suleiman, M. T., N. Lusu, and A. Raich. 2014. "Development of pervious concrete pile ground-improvement alternative and behavior under vertical loading." *J. Geotech. Geoenviron. Eng.* 140 (7): 04014035. [https://doi.org/10.1061/\(ASCE\)GT.1943-5606.0001135](https://doi.org/10.1061/(ASCE)GT.1943-5606.0001135).
- Thakur, A., S. Rawat, and A. K. Gupta. 2021a. "Experimental study of ground improvement by using encased stone columns." *Innovative Infrastruct. Solutions* 6 (1): 1–13. <https://doi.org/10.1007/s41062-020-00383-y>.
- Thakur, A., S. Rawat, and A. K. Gupta. 2021b. "Experimental study of ground improvement by using encased stone columns." *Innovative Infrastruct. Solutions* 6 (1): 1–17. <https://doi.org/10.1007/s41062-020-00383-y>.
- Thakur, A., S. Rawat, and A. K. Gupta. 2021c. "Experimental and numerical investigation of load-carrying capacity of vertically and horizontally reinforced floating stone column group." *Geotech. Geol. Eng.* 39 (4): 3003–3018. <https://doi.org/10.1007/s10706-020-01674-y>.
- Wood, D. M., W. Hu, and D. F. T. Nash. 2000. "Group effects in stone column foundations: Model tests." *Géotechnique* 50 (6): 689–698. <https://doi.org/10.1680/geot.2000.50.6.689>.
- Yu, F., D. Sun, J. Wang, and M. Hu. 2019. "Influence of aggregate size on compressive strength of pervious concrete." *Constr. Build. Mater.* 209: 463–475. <https://doi.org/10.1016/j.conbuildmat.2019.03.140>.
- Zhang, J., X. Cui, D. Huang, Q. Jin, J. Lou, and W. Tang. 2016. "Numerical simulation of consolidation settlement of pervious concrete pile composite foundation under road embankment." *Int. J. Geomech.* 16 (1): 1–10. [https://doi.org/10.1061/\(ASCE\)GM.1943-5622.0000542](https://doi.org/10.1061/(ASCE)GM.1943-5622.0000542).
- Zhang, J., X. Cui, R. Lan, Y. Zhao, H. Lv, Q. Xue, and C. Chang. 2017. "Dynamic performance characteristics of pervious concrete pile composite foundations under earthquake loads." *J. Perform. Constr. Facil.* 31 (5): 04017064. [https://doi.org/10.1061/\(ASCE\)CF.1943-5509.0001056](https://doi.org/10.1061/(ASCE)CF.1943-5509.0001056).
- Zhang, L., and M. Zhao. 2015. "Deformation analysis of geotextile-encased stone columns." *Int. J. Geomech.* 15 (3): 04014053. [https://doi.org/10.1061/\(ASCE\)GM.1943-5622.0000389](https://doi.org/10.1061/(ASCE)GM.1943-5622.0000389).